Aerodynamic aspects of the sealing of gas-turbine rotor-stator systems

Part 1: The behavior of simple shrouded rotating-disk systems in a quiescent environment

U. P. Phadke
Scientific Generics, King's Court, Cambridge CB4 2PF, UK

J. M. Owen
School of Engineering and Applied Sciences, University of Sussex, Falmer, Brighton, Sussex BN1 9QT, UK

Received 3 April 1987 and accepted for publication on 29 June 1987

The sealing characteristics of a shrouded rotor-stator system have been studied using flow visualization, pressure, and concentration measurements. Seven shroud geometries, incorporating axial clearance, radial clearance, or mitered seals, have been tested for a range of clearance ratios and rotational Reynolds numbers up to $Re_\theta = 1.2 \times 10^6$. For all axial clearance seals, the superimposed airflow rate necessary to prevent the ingress of external fluid into the rotor-stator wheel space increased with rotational speed and with seal clearance. Owing to a "pressure inversion effect," where the pressure in the wheel space increased rather than decreased with rotational speed, the increase of sealing flow rate with rotational speed for two of the radial clearance seals was less than that for the other seals. As expected, the mitered seal had a performance intermediate between the purely axial clearance seals and the radial clearance seals exhibiting the pressure inversion effect. The tests referred to above were conducted in a quiescent environment. In Parts 2 and 3, the effect of an external axial flow of air at the periphery of the system is studied.

Keywords: sealing; rotating disks; rotor-stators

Introduction

In the advanced gas-turbine engine, the high-pressure turbine disks are cooled by a radially outward flow of air extracted from the compressor (Figure 1). This air removes heat conducted into the disk from the turbine blades and prevents the ingress of hot mainstream gas into the wheel space between the rotating disk and the adjacent stationary casing. To minimize the cooling air required to prevent ingress, seals are fitted near the periphery of the wheel space: cooling air flows out through the small clearances between the rotating and stationary components of these seals.

To improve engine efficiency, the use of cooling air is kept to a minimum; the subject of disk sealing has become of increasing interest to the gas-turbine designer[1-3]. However, the geometric complexity of gas-turbine disks and seals makes a fundamental investigation difficult, and insight is usually gained by studying simple, plane, rotating-disk systems[4]. The particular system considered in this paper is the so-called shrouded rotor-stator system, an example of which is shown in Figure 2.

If a disk rotates at sufficiently high speed inside a stationary cylindrical casing, in the absence of a superimposed flow, fluid moves radially outward in the disk boundary layer and inward in the stator boundary layer. Between the boundary layers, a core of fluid rotates at the speed necessary to satisfy the conservation of mass and momentum. This rotation creates a radial pressure gradient so that the pressure in the wheel space increases with radius.

If there is a small clearance between the cylindrical casing (or shroud) and the rotor, as shown in Figure 2, then some of the fluid in the rotor boundary layer is "pumped" out of the system. The outflow is compensated by an equivalent inflow of external fluid: this is referred to as *ingress*. Ingress can be prevented by supplying a superimposed radial outflow of fluid, which creates a radial pressure drop across the clearance between the shroud and the rotor. The superimposed flow then "pressurizes" the wheel space and can prevent ingress.

Bayley and Owen[5] studied such a system in which there was a

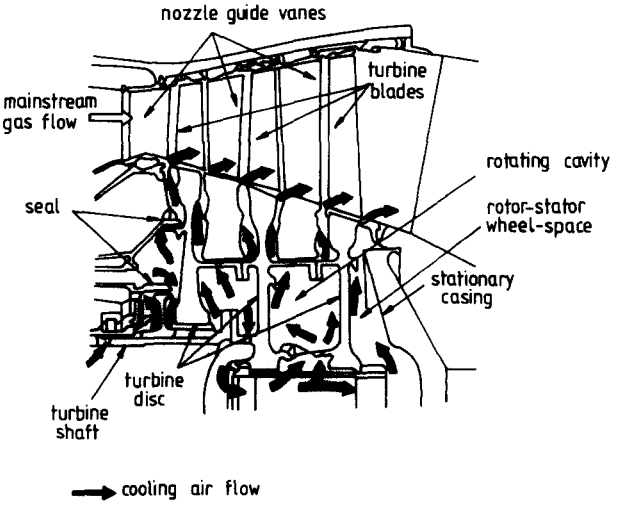

Figure 1 An air-cooled gas turbine rotor

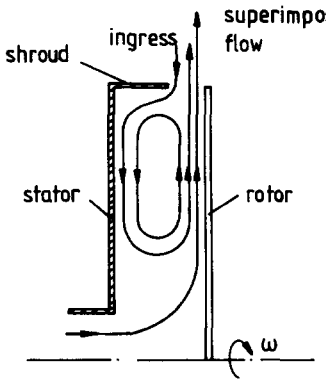

Figure 2 Schematic diagram showing ingress in a shrouded rotor-stator system with an axial clearance seal

small axial clearance, s_c, between the stationary shroud and the rotor. Assuming that viscous effects were small, they showed, from theoretical considerations, that the minimum dimensionless flow rate necessary to prevent ingress, $C_{w,min}$, should be related to the dimensionless clearance, G_c, and the rotational Reynolds number, Re_θ, by

$$C_{w,min} = CG_c Re_\theta \quad (1)$$

where $C_{w,min}$, G_c, and Re_θ are defined in the Nomenclature. They conducted experiments for rotor-stator gap ratios of $G=0.06$, 0.12, and 0.18 and shroud clearance ratios of $G_c=0.0033$ and 0.0067 for rotational Reynolds numbers up to $Re_\theta = 4\times10^6$. The static pressure on the stator near the outer part of the wheel space was used to determine ingress: subatmospheric pressures on the stator were associated with ingress; positive pressures were taken to signify a sealed system. A value of $C=0.61$ in Equation 1 was used to correlate their results.

The present authors[6] extended the study of sealing for axial clearance seals, using both flow visualization and pressure measurements to determine $C_{w,min}$ for five clearance ratios in the range $0.0025 \leqslant G_c \leqslant 0.04$ and $G=0.1$. From the flow visualization, they obtained the correlation for $Re_\theta \leqslant 10^6$:

$$C_{w,min} = 0.14 G_c^{0.66} Re_\theta \quad (2)$$

In subsequent investigations with radial clearance seals[7,8], they reported a "pressure inversion effect" in which, above a certain flow rate, the pressure in the wheel space increased rather than decreased with increasing rotational speed. As a consequence, the radial clearance seals were found to require a smaller value of $C_{w,min}$ than was necessary for the equivalent axial clearance seals.

A recent study[9] has been conducted in which "blade-cooling" air, supplied through preswirl nozzles near the periphery of the stator, was used in conjunction with "disk-cooling" air, supplied from the center of the stator. Double-mitered seals were fitted, which, like the radial clearance seals referred to above, could produce a pressure inversion effect. It was found that more air was needed to seal the system if both cooling flows were supplied simultaneously than if either flow was supplied separately. The authors also made concentration measurements to determine the mixing that occurred between the blade-cooling and disk-cooling air.

The above investigations were carried out in a "quiescent environment." In a gas turbine, there is an axial flow of mainstream gas across the outlet of the seals, and this can have a significant effect on seal performance. The object of this three-part series of papers is to provide data and to give some insight into the performance of a variety of rotor-stator seals with and without an external flow of fluid. In Part 1, the flow structure and performance of seven seals operating in a quiescent environment are discussed. In Parts 2 and 3 (referred to hereafter as II and III), the effects of quasi-axisymmetric and nonaxisymmetric external flows on the sealing characteristics are considered.

Experimental apparatus

Introduction

The experimental work reported in this paper was conducted on two different rotating-disk rigs, both with the same nominal dimensions chosen to provide half-scale simplified models of real gas-turbine-disk systems. In the initial stages of the investigation, a basic rotor-stator rig, described below, was used to study the behavior of rotor-stator systems in a quiescent environment. A separate experimental facility for studying rotor-stator systems in the presence of external peripheral flows was also designed and constructed. This "external flow rig," which was used for some quiescent environment tests, is

Nomenclature

C_{ij}	Ingress constant
C_w	$\dot{m}/\mu r_0$, mass flow coefficient
G	s/r_0, gap ratio
G_c	s_c/r_0, seal clearance ratio
H	z_0/r_0, seal overlap ratio
$\dot{m}$	Mass flow rate of sealing air
p	Static pressure
p^*	$10^3(p-p_a)/p_a$, dimensionless pressure drop
r	Radial distance from disk centerline
r_0	Outer radius of disk
Re_θ	$\rho\omega r_0^2/\mu$, rotational Reynolds number
s	Axial gap between rotor and stator
s_c	Seal clearance
V_r, V_θ, V_z	Radial, tangential, and axial components of velocity
x	r/r_0 dimensionless radial distance
z	Axial distance measured from stator face
z_0	Axial overlap of radial clearance seals
μ	Fluid viscosity
ρ	Fluid density
ω	Angular speed of rotor
η	Volumetric concentration (ratio of volumetric flow rates of nitrous oxide and air)

Subscripts

a	Ambient conditions
c	Coolant flow
e	External flow
i	($i=1,\ldots,7$) seal type
j	($j=1,2$) ingress criterion
min	Minimum value to prevent ingress
r	Rotor
s	Stator
1,2	Outer and inner shrouds, respectively

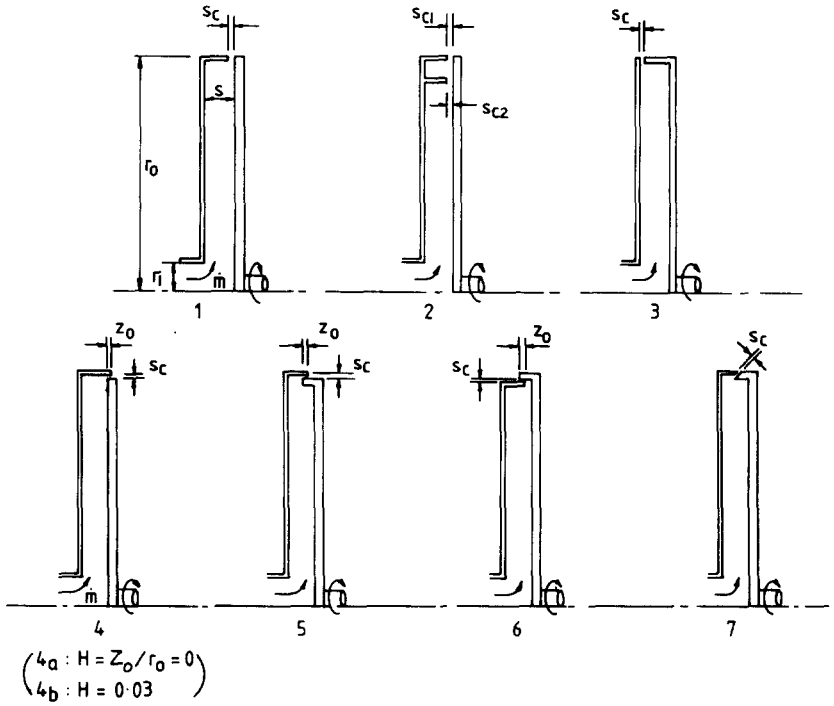

Figure 3 Schematic diagram of the seven seal geometries

described in II, and a schematic diagram of the rig and instrumentation is shown in Figure 2 of II.

For the tests in a quiescent environment reported here, however, both rigs were essentially similar. For a more detailed description of the two rigs, see Ref. 10.

The basic rig

The rotor-stator system comprised a rotating disk made from aluminum alloy and a stationary disk made from perspex. Peripheral shrouds could be attached to the rotor and the stator, and the nominal diameter of the resulting rotor-stator cavity was approximately 380 mm, depending on the shroud configuration. A superimposed flow of "cooling" air entered the cavity through a hole of 38 mm diameter in the center of the stator and left through the clearance between the rotating and stationary shrouds. Seven shroud geometries, which are shown in Figure 3, were tested for clearance ratios in the range $0.0025 < G_c < 0.04$. Two different overlap ratios were used with seal 4: for seal 4a, $H = 0$; for 4b, $H = 0.03$. For seals 5 and 6, $H = 0.01$. For the double-shrouded seal 2, the ratio of the radii of the inner and outer shrouds was 0.9.

Two different types of rotor were used: a plane rotor consisting of a single aluminum alloy disk 6 mm thick, and a composite rotor made from two aluminum alloy disks with a perspex or aluminum shroud sandwiched between. Rotational speeds up to 4000 r/min were achieved using a variable-speed electric motor that was attached by pulleys and belt to the rotor shaft. Growth in the outer radius of the composite disk at high rotational speeds could reduce the clearance when the radial clearance seals were tested. Estimated and measured radial growth confirmed that at 4000 r/min the reduction in clearance for the smallest radial clearance ratio tested ($G_c = 0.0025$) was less than 5%.

The stator was made from a perspex disk 10 mm thick to the back of which were attached four orthogonal radial supports made from aluminum of 19 mm axial depth and 12.7 mm transverse width. A perspex shroud of 2 mm thickness could be secured to the periphery of the stator by a retaining ring. Shrouds of various axial widths were used to create different axial clearances, and annular spacers were used to alter the radial clearances. The stator could be moved axially with respect to the rotor, but for the tests described below a gap ratio of $G \simeq 0.1$ was used.

The sealing air was supplied from a centrifugal fan with an output up to 0.08 m^3/s at 600 mm WG. The air entered the rotor-stator cavity through a pipe of 38 mm inside diameter and 1.2 m length.

Instrumentation

The rotor speed was measured to an accuracy of ± 1 r/min by a digital tachometer. The coolant flow rate was measured to an estimated accuracy of $\pm 3\%$ by an Annubar differential pressure meter and a TDM micromanometer.

The stator was fitted with static-pressure taps of 0.25 mm diameter on four orthogonal radii. Static-pressure taps were also located on the inner and outer circumferential surfaces, and on the radial face next to the rotor, of some of the stationary shrouds. The pressure measurements were made with a Mercury M10 electromanometer (resolution 0.05 mm WG, and with an auto-zero facility) and a manually operated bank of pressure switches.

Flow visualization of the rotor-stator cavity was achieved by injecting smoke into the cooling air, or into the external air, and using a laser to provide slit illumination. Dense clouds of micron-sized oil particles were produced by a Concept smoke generator. The slit illumination was created using either a 5-mW He-Ne laser or, for photographic purposes, a 4-W Ar-ion laser, both of which were used in conjunction with cylindrical and collimating lenses. Photographs were taken with a Canon A1 camera (operating in the "aperture-preferred" mode), the axis of the camera lens being normal to the plane of illumination. Video recordings were made by a Sony video camera, monitor, and

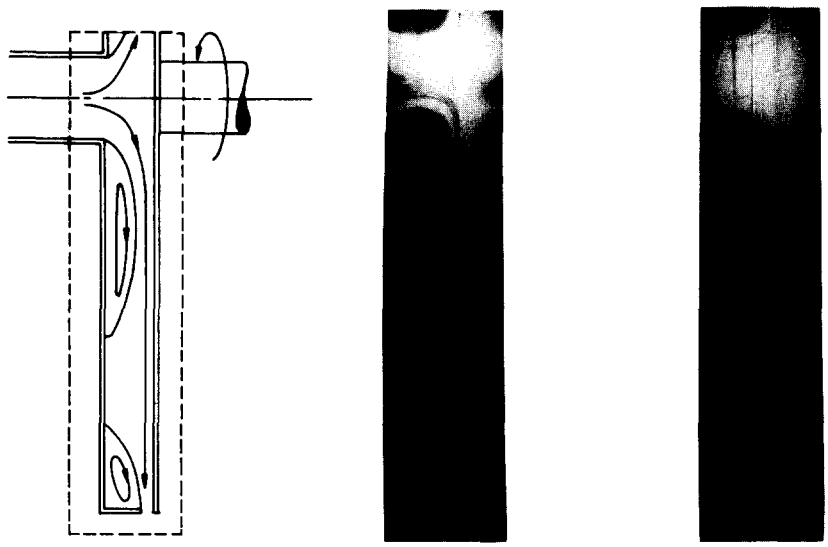

(a) field of view (b) $C_w = 280$ (c) $C_w = 400$

Figure 4 Flow visualization for seal 1 with $G_c = 0.01$ and $Re_\theta = 5 \times 10^4$

tape recorder, with slow-motion playback facilities. Additional details of the flow visualization techniques are given in Refs. 11 and 12.

Velocity and concentration measurements in the rotor-stator wheel space were made with a two-hole transverse-cylinder probe of 3.2 mm OD, which was moved axially and rotated by a computer-controlled traversing table. For velocity measurements, the probe pressures were measured by the electromanometer. For concentration measurements, several hundred parts per million of nitrous oxide were injected into either the sealing air or the external air, and isokinetic samples, extracted from the wheel space by a sampling pump connected to one hole of the transverse-cylinder probe, were analyzed by a GP Instrumentation IRGA 120 infrared gas analyzer. Further details of this system and its validation are given in Ref. 13.

Ingress criteria: the determination of $C_{w,min}$

The three different techniques used to detect ingress, based on pressure measurements, flow visualization, and concentration measurements, are described below.

The static pressure on the stator gives an indication of whether the wheel space is sealed: ingress is associated with negative pressures (that is, the pressure in the wheel space is lower than that of the external fluid). A problem arises, however, in the quantification of this phenomenon: as the pressure varies with radius, at what location will a zero pressure indicate incipient ingress? The question can only be answered by comparing the pressure technique with the concentration and flow visualization techniques. From such comparisons, it was found that the static pressure measured on the surface of the stator at a radial location of $r/r_0 \simeq 0.97$ produced values of $C_{w,min}$ that were reasonably consistent with, although slightly higher than, those of the other techniques. Although it provided only an indirect measurement of $C_{w,min}$, the pressure technique has the virtue of experimental simplicity.

For the flow visualization technique, smoke was injected at the periphery of the illuminated cavity. When the sealing flow rate was sufficiently low, ingress occurred and smoke entered the cavity. With the rotational speed held constant, the flow rate was increased until no smoke could be seen to enter, and hence $C_{w,min}$ was determined. Although not a precise technique, results repeated at different times by different research workers showed no systematic variations. However, ingress was much more difficult to see in those tests with the smaller clearance ratios.

In the concentration technique, nitrous oxide was injected into the sealing flow so that a mixture of known concentration entered the wheel space. With the flow rate held constant, the rotational speed was increased until the concentration, measured with the transverse-cylinder probe, began to decrease. This decrease was caused by the sealing-flow mixture being diluted with ingested "fresh" air, and hence $C_{w,min}$ could be readily determined. Like the pressure technique, quantification depended on the location of the probe.

Performance of the datum axial clearance seal (seal 1)

Using flow visualization, we investigated the structure of the flow for the datum seal (seal 1 in Figure 3). For laminar flow, the structure was easy to visualize, and good photographic evidence of the flow patterns was obtained. For turbulent flow, the patterns were more difficult to identify, and no useful photographs could be obtained.

Figure 4 shows one of the results obtained for seal 1 with laminar flow for $G_c = 0.01$, $Re_\theta = 5 \times 10^4$, and $C_w \simeq 280$ and 400. The sealing flow enters near the top left-hand side of the photograph and leaves near the bottom right-hand side; note that reflections cause mirror images near the surfaces of the rotor and stator. The incoming flow attaches to the rotor, forming a boundary layer in which there are small wavelike instabilities for $x \geqslant 0.45$, and the recirculating flow near the stator shows larger instabilities. A broadly similar structure was also observed for turbulent flow.

Figure 5 shows the effect of C_w and Re_θ on the radial distribution of pressure for $G_c = 0.01$. The pressure in the wheel space tends to increase with increasing flow rate and with decreasing rotational speed. For $C_w = 1490$, the rotation causes the pressure in the wheel space to become negative with respect to the external pressure. For $C_w = 11{,}900$, however, although there is a monotonic decrease in pressure with rotational speed, the pressure in the cavity still remains positive at $Re_\theta = 10^6$. For

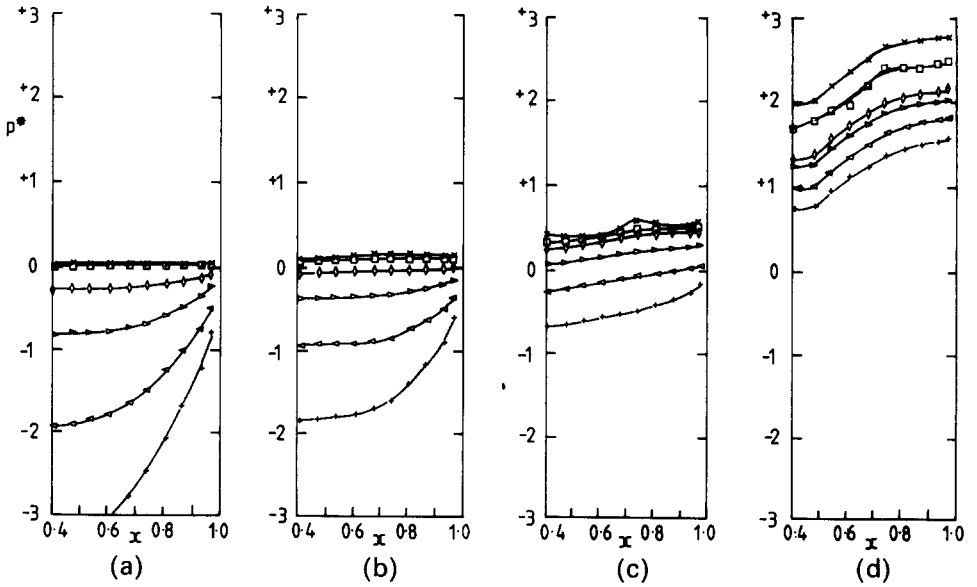

Figure 5 The effect of C_w and Re_θ on the radial distribution of static pressure for seal 1 with $G_c=0.01$: (a) $C_w=1490$; (b) $C_w=2950$; (c) $C_w=5940$; (d) $C_w=11{,}900$

$Re_\theta/10^6$	0	0.2	0.4	0.6	0.8	1.0
Symbol	×	□	◇	▷	◁	+

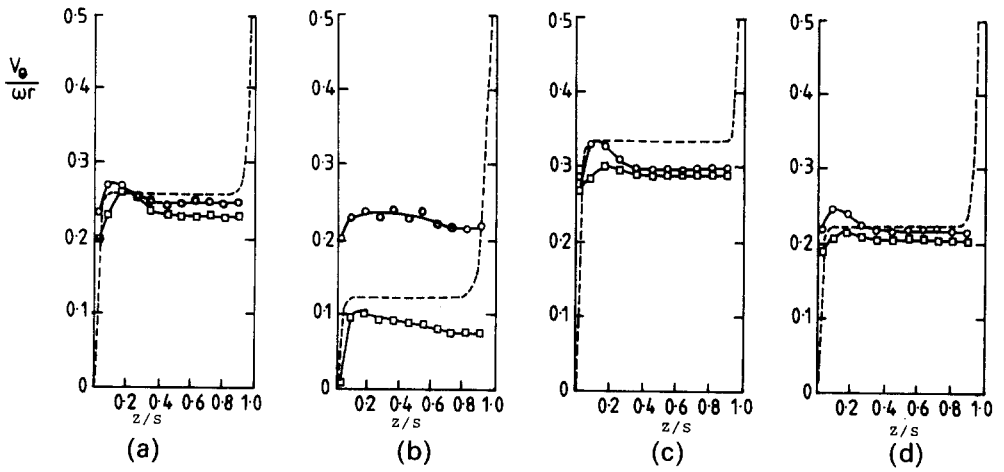

Figure 6 The effect of G_c, C_w, and Re_θ on the axial distribution of tangential velocity at $x=0.81$ for seal 1. Experimental data: ○, $G=0.01$; $G_c=0.005$; ----, Equation 3: (a) $C_w=1490$, $Re_\theta=0.5\times10^6$; (b) $C_w=2950$, $Re_\theta=0.5\times10^6$; (c) $C_w=1490$, $Re_\theta=10^6$; (d) $C_w=2905$, $Re_\theta=10^6$

a given value of C_w, there is a critical Reynolds number at which the pressure in the wheel space changes from positive to negative, after which ingress of external fluid into the cavity occurs.

The axial variations of the measured tangential component of velocity for various values of G_c, C_w, and Re_θ at $x=r/r_0=0.81$ are shown in Figure 6. Also included are theoretical curves obtained by Owen[14] from approximate solutions of the momentum-integral equations. In the core of fluid between the boundary layers on the rotor and stator, the tangential component of velocity, $\bar{V}_\theta$, can be calculated, according to Ref. 14, by

$$(1-\beta)^{8/5}(1-0.51\beta)-0.638\beta^{4/5}=4.57C_w\,Re_\theta^{-4/5}x^{-13/5} \quad (3)$$

where $\beta=\bar{V}_\theta/\omega r$. For $C_w=0$, $\beta=0.426$, and $\beta=0$ when

$$C_w=0.219Re_\phi^{4/5}x^{13/5} \quad (4)$$

which is the entrainment rate predicted by von Karman[15] for turbulent flow over a free disk. Thus, according to Equation 4, the core rotation is suppressed (and radial inflow on the stator is prevented) when the superimposed flow rate is equal to that entrained by a free disk.

Figure 6 shows that, for most of the results, the approximate solution is in reasonable agreement with the measured velocities. The solution takes no account of shroud clearance ratio and, apart from the results shown in Figure 6(b), G_c has only a small effect on the measured values: no explanation can be offered for the large difference between the two sets of experimental data in Figure 6(b). The peaks in the velocity measurements near the stator have also been observed by other research workers: as pointed out in Ref. 14, the oscillation in the flow near the stator is consistent with Ekman-layer flow.

Figure 7 shows the axial variation of $(\eta-\eta_c)/\eta_c$ (where η and η_c are the volumetric concentrations of nitrous oxide in the wheel space and in the cooling air at the inlet to the system, respectively) at $x=0.81$ for different values of G_c, C_w, and Re_θ.

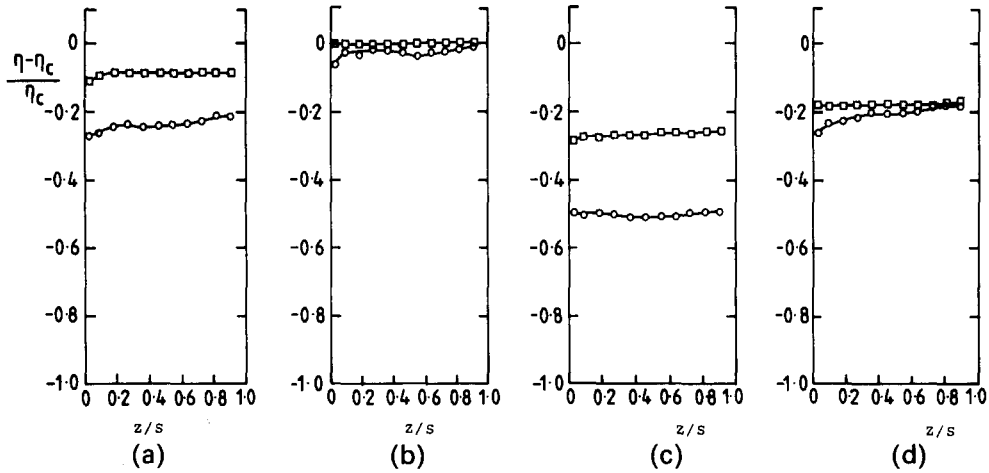

Figure 7 The effect of G_c, C_w, and Re_θ on the axial distribution of concentration at $x=0.81$ for seal 1. Experimental data: ○, $G_c=0.01$; □, $G_c=0.005$: (a) $C_w=1490$, $Re_\theta=0.5\times10^6$; (b) $C_w=2950$, $Re_\theta=0.5\times10^6$; (c) $C_w=1490$, $Re_\theta=10^6$; (d) $C_w=2950$, $Re_\theta=10^6$

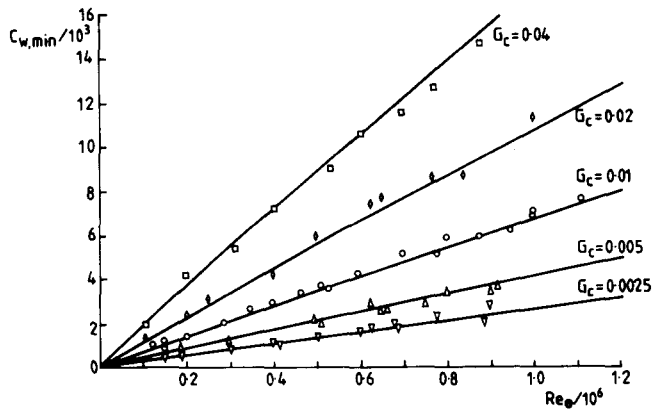

Figure 8 The effect of G_c on the variation of $C_{w,min}$ with Re_θ obtained by flow visualization for seal 1:

G_c	0.0025	0.005	0.01	0.02	0.04
Symbol	▽	△	○	◇	□

——— Equation 5: $C_{m,min}=0.280G_c^{0.677}Re_\theta^{0.956}$

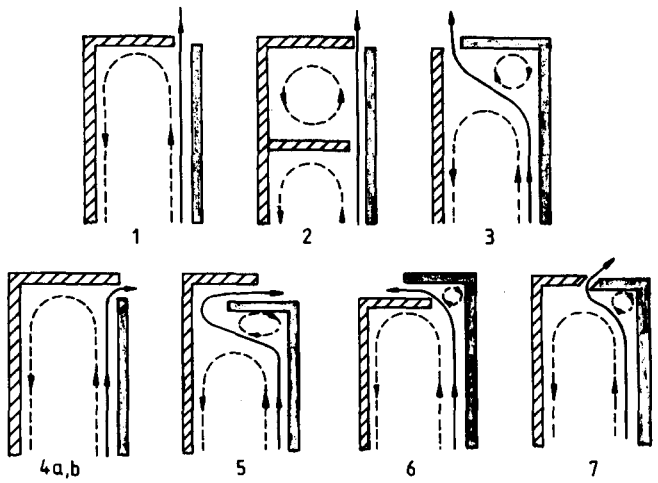

Figure 9 Simplified representation of flow patterns near the outlet of each of the seven seals. ——▶——=superimposed flow; — — ▶— — —=secondary flow

Table 1 Correlation constants for Equation 5

	j \ i	1	3	4a	4b	5	6	7
C_{ij}	1	0.280	0.143	0.091	0.0189	0.0224	0.188	0.042
	2	0.197	0.114	0.076	0.0208	0.028	0.149	0.039
m_{ij}	1	0.677	0.542	0.482	0.199	0.229	0.620	0.338
	2	0.604	0.500	0.473	0.274	0.291	0.580	0.361
n_{ij}	1	0.956	0.956	0.950	0.930	0.951	0.951	0.950
	2	0.956	0.955	0.950	0.930	0.949	0.950	0.951

i=seal number (see Figure 3); j=1: flow visualization data; j=2: pressure criterion data.

Ingress of "fresh" unseeded air into the wheel space causes a dilution of the seeded air such that $(\eta-\eta_c)/\eta_c<0$. Note that only for $G_c=0.005$, $C_w=2950$, and $Re_\theta=0.5\times10^6$ is the wheel space sealed. Ingress occurs in all other cases, and the amount of ingested fluid increases with increasing Re_θ and G_c and with decreasing C_w. Also note that, like the velocity distribution, there is little axial variation of concentration in the core between the boundary layers on the rotor and stator.

Figure 8 shows the effect of G_c on the variation of $C_{w,min}$ with Re_θ obtained from flow visualization. $C_{w,min}$ increases with G_c and, for all values of G_c, $C_{w,min}$ increases nearly linearly with Re_θ. In order to correlate the data, a generalized power-law relationship of the following form was assumed:

$$C_{w,min}=C_{i,j}G_c^{m_{i,j}}Re_\theta^{n_{i,j}} \qquad (5)$$

where the subscript i refers to the seal type (1, 2, 3, etc.) and j refers to the ingress criterion ($j=1$ for flow visualization, $j=2$ for pressure). The values of the constants $C_{i,j}$, $m_{i,j}$, and $n_{i,j}$ were obtained by multiple-regression analysis, based on minimizing the least-squares errors. The calculated values are given in Table 1.

Comparative performance of the seven seals

A simplified representation of the streamlines near the outlet of the seven seals is shown in Figure 9. The streamlines were observed or deduced from flow visualization studies at relatively low flow rates and rotational speeds ($C_w\leqslant500$, $Re_\theta\leqslant15^5$).

In all cases, the sealing air entered axially through the central hole in the stator, impinged on the rotor, and flowed outward as a radial wall jet. A separation bubble (not shown in the figure)

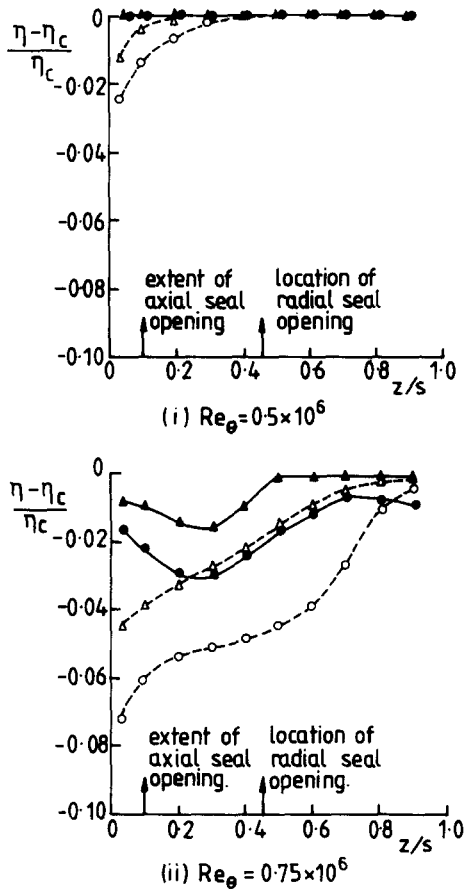

Figure 10 The effect of Re_θ on the distribution of concentration for $G_c=0.01$ and $C_w=2850$. Experimental data: ▲, $x=0.81$; ●, $x=0.94$. Closed symbols refer to seal 5, open symbols to seal 3

occurred near the inlet, and secondary flow (shown by the dotted lines) inside the wheel space resulted in a radial inflow on the stator. Most of the features shown in Figure 9 are self-explanatory, but points that are considered to be important are discussed below.

For seal 2, a strong toroidal vortex formed in the chamber between the two shrouds. For cases where the clearance for the outer shroud was greater than that for the inner one, the first sign of ingress appeared in the chamber between the shrouds. The ingested fluid did not immediately penetrate the inner wheel space.

The flow visualization for seals 4a and 4b was the hardest to observe. The outward flow on the rotor formed a radial jet that impinged on the stationary shroud: the secondary flow traveled across the shroud and moved radially inward on the stator, and the sealing air left via the radial clearance between the shroud and the rotor. When ingress occurred, the radial jet viewed in the r-θ plane was seen to be nonaxisymmetric and unsteady. Increasing the flow rate prevented ingress and stabilized the flow.

In seal 5, the flow separated from the rotor immediately upstream of the rotating shroud, and the resultant jet impinged on the stator. As for seal 4, when ingress occurred, the jet was nonaxisymmetric and unsteady.

The "impinging jet phenomenon" observed for seals 4 and 5 was not seen for seal 6, the other radial clearance seal. The radially outward flow on the rotor separated just upstream of the shroud in a similar way to that observed for seal 3. Seal 7, the mitered seal, showed some evidence of the impinging jet phenomenon, but otherwise it was similar to seal 3.

The impinging jet phenomenon is believed to be the explanation for the pressure inversion effect observed for seals 4 and 5 in Refs. 7 and 8. Unlike other seals, in which the pressure in the cavity decreased with increasing rotational speed, seals 4 and 5 could exhibit the reverse effect: above a certain flow rate, the pressure near the outer part of the wheel space actually increased with increasing speed. This improves the sealing effectiveness: the impinging jet forms a circular "curtain" of fluid that increases the pressure in the outer part of the wheel space and helps to prevent ingress.

Concentration measurements provide additional evidence that ingested fluid moves radially inward near the stator before being entrained by the boundary layer on the rotor. Figure 10 shows the axial variation of $(\eta-\eta_c)/\eta_c$ at $x=0.81$ and 0.94 for seals 3 and 5 with $G_c=0.01$, $C_w=2850$, and $Re_\theta/10^6=0.5$ and 0.75. A negative value of $(\eta-\eta_c)/\eta_c$ indicates that ingress has occurred, which is the case for all tests except those with seal 5 at the lower value of Re_θ. For both seals, the minimum concentration (or maximum "dilution") occurs near the seal opening, and the concentration is much lower near the stator than it is near the rotor. In fact, $(\eta-\eta_c)/\eta_c=0$ near the rotor at $x=0.81$, which suggests that only a small amount of the ingested air reaches the surface of the rotor.

The variation of $C_{w,min}$ with Re_θ, for $Re_\theta<1.2\times10^6$, was obtained for each seal from both the flow visualization and the pressure criterion. For seals 1 and 3, results were obtained for $G_c=0.0025$, 0.005, 0.01, 0.02, and 0.04; for seals 4a, 4b, 5, and 6, $G_c=0.005$, 0.01, and 0.02; for seal 7, $G_c=0.005$ and 0.01. The data for these seals were correlated using Equation 5, and the constants are given in Table 1. For the inner cavity of seal 2, the results for seal 1 may be used if $C_{w,min}$, G_c, and Re_θ are based on the radius of the inner shroud.

Figure 11 shows the variation of $C_{w,min}$ with Re_θ obtained by flow visualization for the seals with $G_c=0.01$. As well as the experimental data, Equation 5 is also plotted. It can be seen that seals 4b, 5, and 7 are the most effective: these seals all exhibited the impinging jet and pressure inversion effects. In particular, seal 4b requires the smallest amount of sealing air; it also exhibits the most nonlinear behavior, with the rate of $C_{w,min}$ decreasing with increasing Re_θ.

The "order of merit" of the seals for $G_c=0.01$ and 0.02 was 4b,

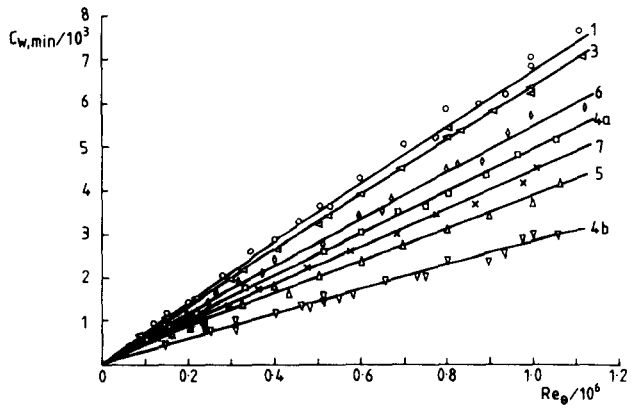

Figure 11 The variation of $C_{w,min}$ with Re_θ obtained by flow visualization for the seals with $G_c=0.01$:

Seal number	1	3	4a	4b	5	6	7
Symbol	○	◁	□	▽	△	◇	×

——— Equation 5 ($j=1$)

5, 7, 4a, 6, 3, and 1. For $G_c = 0.005$, the order was the same, except that seal 1 was slightly more effective than seal 3. The overlapping radial seal 4b requires far less sealing air than the axial clearance seals, and this difference increases with both increasing G_c and increasing Re_θ.

Conclusions

Flow visualization, pressure, and concentration measurements have been used to study the sealing characteristics of a shrouded rotor-stator system operating in a quiescent environment. Seven shroud geometries were tested: three axial clearance, three radial clearance, and a mitered seal. Tests were carried out at a rotor-stator gap ratio of $G = 0.1$ for a range of shroud clearance ratios and for rotational Reynolds numbers of up to $Re_\theta = 1.2 \times 10^6$. To simulate conditions inside an air-cooled gas-turbine rotor, a radial outflow of air was supplied. The air entered the rotor-stator cavity through a hole in the center of the stator and left through the seal clearance between the peripheral shrouds.

For all seals, the flow rate necessary to prevent the ingress of external air into the wheel space increased with increasing rotational speed and with increasing seal clearance. It was shown in earlier work that two of the radial clearance seals could exhibit a pressure inversion effect, where the pressure in the wheel space increased rather than decreased with increasing rotational speed. In this paper, flow visualization was used to show that the pressure inversion effect was associated with radially outward flow on the rotor impinging on either the shroud or the stator. The impingement created a fluid curtain that helped to prevent ingress and made the radial clearance seals more effective than their axial clearance counterparts. For each of the seals, a simple correlation was obtained from which the minimum flow rate necessary to prevent ingress could be determined in terms of the shroud clearance and rotational speed.

Tests have also been conducted for the case where air flows axially over the periphery of the shrouded rotor-stator system. The results of these tests, which are intended to simulate more closely the conditions that occur inside gas-turbine rotors, are presented in II and III.

References

1 Moore, A. Gas turbine internal air systems: a review of the requirements and problems. Paper No. 75-WA/GT-1, ASME Winter Annual Meeting, Houston, Texas, 1975

2 Campbell, D. A. Gas turbine disc sealing system design. AGARD-CP-237, p. 18-1, 1978

3 Suo, M. Turbine cooling. In *The Aero-Thermodynamics of Aircraft Gas Turbine Engines*, ed. G. C. Oates, AFOSR-75-2783, 1978

4 Owen, J. M. Fluid flow and heat transfer in rotating disc systems. In *Heat and Mass Transfer in Rotating Machinery*, eds. D. E. Metzger and N. H. Afgan, Hemisphere, Washington, D.C., 1984

5 Bayley, F. J. and Owen, J. M. The fluid dynamics of a shrouded disc system with a radial outflow of coolant. *J. Eng. Power*, 1970, **92**, 335

6 Owen, J. M. and Phadke, U. P. An investigation of ingress for a simple shrouded rotating disk system with a radial outflow of coolant. Paper No. 80-GT-49, 25th Int. ASME Gas Turbine Conf., New Orleans, 1980

7 Phadke, U. P. and Owen, J. M. An investigation of ingress for an air-cooled shrouded rotating disc system with radial clearance seals. *J. Eng. Power*, 1983, **103**, 178

8 Phadke, U. P. and Owen, J. M. The effect of geometry on the performance of "air-cooled" rotor-stator seals. 15th CIMAC Congress, Paris, 1983

9 El-Oun, Z., Neller, P. H., and Turner, A. B. An experimental investigation of ingress in a shrouded rotor-stator system with pre-swirled coolant. Paper No. 87-GT-72, 32nd Int. ASME Gas Turbine Conf., Anaheim, 1987

10 Phadke, U. P. Aerodynamic aspects of the sealing of gas turbine rotor-stator systems. D. Phil. thesis, University of Sussex, 1982

11 Owen, J. M. and Pincombe, J. R. The use of optical techniques in the interpretation of heat transfer measurements. AGARD-CP-281, p. 15-1, 1980

12 Phadke, U. P. Flow visualization in a simple rotor-stator system with throughflow. Proc. 3rd Int. Symp. on Flow Visualization, Hemisphere, Washington, D.C., Springer-Verlag, New York, 1983

13 Downie, J. H. and Phadke, U. P. The development of a microcomputer-controlled probe system for the investigation of velocity and concentration fields in mixing flows with recirculation. Paper A2, Int. Conf. on the Use of Micros in Fluids Eng., London, 1983

14 Owen, J. M. An approximate solution for the flow between a rotating and a stationary disc. To be presented at 33rd Int. ASME Gas Turbine Conf., Amsterdam, 1988

15 von Karman, Th. Uber laminare und turbulente Reibung. *Z. Angew. Math. Mech.*, 1921, **1**, 233